JACS
JOURNAL OF THE AMERICAN CHEMICAL SOCIETY
pubs.acs.org/JACS
Article

Molecular Routes of Coke Species on HZSM-5 Zeolite with Atomic-Resolution Structural Identification

Yingjun He,[#] Yi Zheng,[#] Yiyao Chen, Jing Niu, Jingrui Chen, Guoju Yang, Wenna Zhang, Xianwen Zhang, Shutao Xu, Wenfu Yan, Mengxi Liu,* Yuchun Zhi,* Yingxu Wei, Xiaohui Qiu, and Zhongmin Liu*

Cite This: J. Am. Chem. Soc. 2025, 147, 41379–41389

ABSTRACT: Catalyst deactivation has drawn continuing concern from both the academia and industry. Preventing deactivation and optimizing the regeneration process necessitate molecular deciphering of coke deposits. Key to achieving this goal is to identify previously less unexplored, more condensed coke species. Herein, taking commercially relevant HZSM-5 zeolite-catalyzed methanol-to-hydrocarbon as a prototypical reaction, we decode the "structural code" of the previously elusive coke molecules. This is made possible by integrating multiple techniques, especially scanning tunneling microscopy (STM) and noncontact atomic force microscopy (nc-AFM) techniques, which enables the single-molecule direct imaging of coke species with atomic resolution in real space. Combined with complementary techniques, such as gas chromatograph−mass spectrometry and matrix-assisted laser desorption/ionization Fourier-transform ion cyclotron resonance mass spectrometry, coke species with an explicit molecular structure covering soluble and insoluble ranges are identified. With this, their molecular routes are consequently unveiled. Molecular imaging with atomic precision resolves the previous ambiguity about "average structures" of "ensemble coke" given by the traditional means with group-based structural identification. This work showcases the potential of STM and nc-AFM as powerful mechanistic tools for resolving mechanistic hypotheses in catalysis.

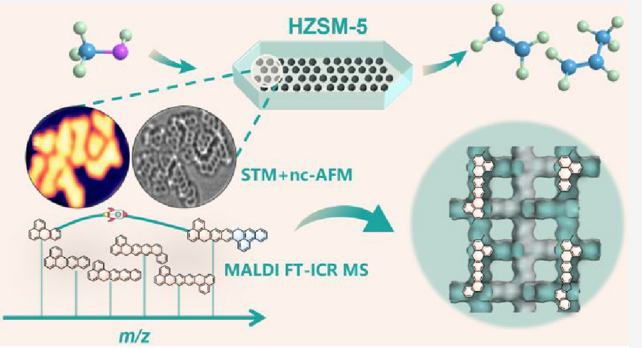

INTRODUCTION

Zeolites are one of the most industrially important crystalline microporous materials. Due to their moderately strong acidities and shape selectivity, zeolites are widely used as solid acid catalysts to mediate chemical reactions in fine chemicals, petroleum- and coal-based chemical processes.[1−3] The hydroxyl groups acting as the Brønsted acid sites, associated with the surrounding confining microporous voids being of molecular dimensions (<2 nm), collectively behave as the actual active centers.[4,5] Nanospace confinement endowed by the molecular-sized confines (nanoenvironments) of zeolites can appreciably accelerate chemical reaction (via stabilizing the reaction transition state) and delicately control the product selectivity (via size and shape selectivity control).[4,6] In the zeolite confined space, coking and deactivation are inevitable. The active organic species residing in the inner and outer surfaces of zeolites gradually grow into inactive polycyclic aromatic hydrocarbons (PAHs), covering the acid sites and hindering the mass transfer, thus eventually terminating the catalysis reaction.[7−10]

Understanding how PAHs deactivate zeolites at the molecular or even atomic scale is of fundamental significance, and also highly relevant to industrial processes.[8,11] Coking is one of the main challenges during industrial operations, especially for reactions with fast coke deposits that severely impair process efficiency. Molecular deciphering of PAHs is the prerequisite for alleviating (or even preventing) deactivation and for improving the catalysis efficiency. Despite intensive research efforts, a unified and complete molecular picture of the full spectrum of coke remains absent and is only beginning to be fully unveiled.[12]

Although a substantial amount of work has dealt with the deactivation of PAHs as the known deactivating species,[8−12] the majority of coke molecules remain uncharacterized, and the molecular structures of those heavier coke species are still less known. These insoluble, heavier coke molecules are highly polyaromatic, with many fused rings. The limited information

Received: June 24, 2025
Revised: October 22, 2025
Accepted: October 22, 2025
Published: October 29, 2025

https://doi.org/10.1021/jacs.5c10664
J. Am. Chem. Soc. 2025, 147, 41379−41389

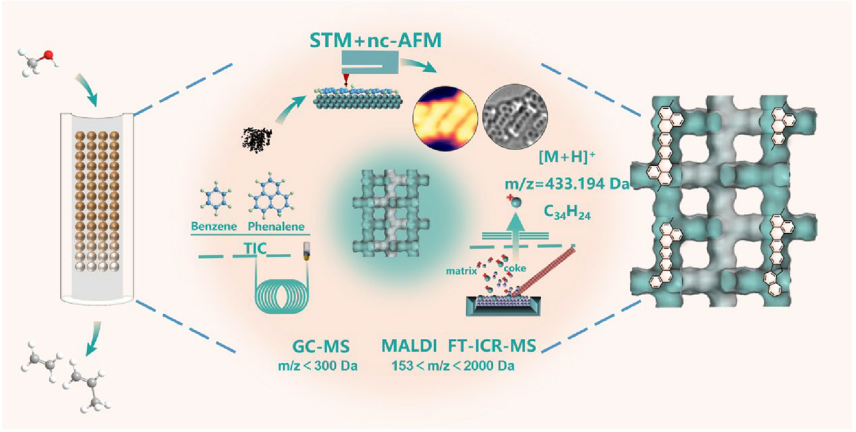

Figure 1. Schematic illustration of the strategy to identify the broad-range molecular structures of coke species by integrating GC−MS, MALDI FT-ICR MS, and STM and nc-AFM techniques.

is often related to their elemental compositions,[13] except for a preliminary proposal of cage-passing molecular structures of the condensed PAHs deduced by MALDI FT-ICR MS over the cage-structured SAPO-34.[12] In this regard, unlocking the "structural coding" of coke species is the prerequisite for unraveling the growth routes of coke. Hence, this work aims to decode the molecular structures of more condensed PAH molecules.

Much effort has been made to identify the molecular identity of those complex PAH molecules. The classic Guisnet's method, i.e., liberating the coke deposits from the spent zeolites by HF dissolution, extracting the released organics with solvent, followed by gas chromatograph−mass spectrometry (GC−MS) analysis, is commonly used to identify the soluble aromatic molecules (up to approximately four rings).[14] This method is proven to be nondestructive, as 20−40% HF will not cause any significant change of aromatic structure,[14] but it fails in identifying the more condensed coke (with molecular weight >300 g/mol). Spectroscopic methods such as IR,[15,16] UV−vis,[15−17] UV-Raman,[18,19] ^{13}C NMR,[16] etc., with the merits of nondestructive and operando operation, can distinguish the lighter aromatic species from the highly condensed constituents.[20] However, such spectroscopic information is generally obtained from bulk analysis. Recently, two advanced microscopic techniques, i.e., confocal fluorescence microscopy (CFM)[21−23] and atom probe tomography (APT),[24,25] were developed by Weckhuysen et al. with sub-μm and sub-nm resolution, respectively. These two advanced microscopic techniques can directly visualize the spatial location of coke species in a single zeolite particle. However, they are unable to provide the detailed molecular structural information and are applicable to large zeolite crystallites (with a size of 50−100 μm).[23,25]

More recently, the single-crystal electron diffraction technique was adopted to directly map the location of coke species inside zeolite channels.[26] The electron diffraction results showed that coke nucleation started in the channel intersections of HZSM-5 and then grew along the straight channel.[26] Besides, the advanced MS techniques, such as MALDI FT-ICR MS with the merits of soft ionization that minimizes fragmentation, have been adopted to fingerprint the molecular structures of heavier PAHs.[12,27,28] MALDI FT-ICR MS can trace the growth trajectory of coke molecules formed inside zeolite pores, but the accurate molecular structures are still difficult to determine only on the basis of m/z signals.[12,27,28]

These spectroscopic and microscopic tools provide rather limited information about the structural details of coke molecules, and they afford information about "average structures" of "ensemble coke" with the group-based structural identification. Thus, fingerprinting coke species at a molecular or subnanometer level, with atomic resolution structural identification, is highly desirable. Noncontact atomic force microscope (nc-AFM) enables real-space visualization of intramolecular chemical bonds with atomic resolution.[29,30] This single-molecule imaging technique has exhibited unique advantages in the analysis of complex organic mixtures, and thus has successfully been applied for direct imaging of PAHs and their derivatives in petroleum asphaltenes,[31,32] interstellar organic haze,[33] combustion soot,[34] etc.

Herein, taking HZSM-5-catalyzed MTH as a model reaction, we combined STM and nc-AFM techniques to directly image coke molecules with atomic resolution. The previously unidentified radical and oxygen-containing species were also imaged. These findings provide structural insights into the molecular mechanisms of coke growth. By integrating STM and nc-AFM with GC−MS and MALDI FT-ICR MS techniques (Figure 1), a molecular picture spanning soluble coke to insoluble one was achieved. With this, a channel intersection-passing deactivation mechanism was proposed on HZSM-5. Direct visualization and identification of coke species resolved the uncertainties about the "hypothetical/average structures" of "ensemble coke" given by traditional tools, bringing new insights into the widely studied catalysis reactions.

RESULTS AND DISCUSSION

Taking Industrially Relevant MTH as a Prototypical Reaction. Since its discovery in 1972, HZSM-5 zeolite has underpinned lots of important processes in coal, chemical, and petrochemical industry, such as MTH, isomerization, transalkylation of aromatics, and fluid catalytic cracking reactions,[35] etc. MTH reaction is autocatalytic, where a pool of olefins, methylcyclopentenyl, and polymethylbenzene species inhibited in zeolite micropores function as actual active centers to catalyze methanol conversion.[36−38] The complex autocatalytic reaction network drives the high turnover of the MTH

https://doi.org/10.1021/jacs.5c10664
J. Am. Chem. Soc. 2025, 147, 41379−41389

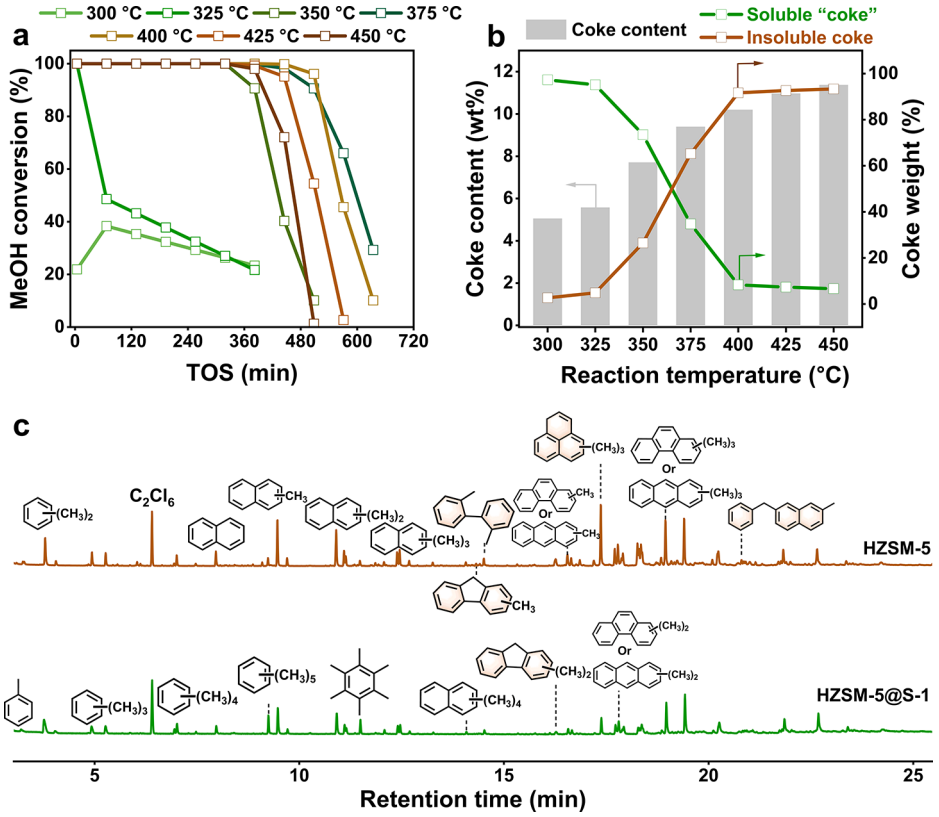

Figure 2. (a) MTH reaction performance of HZSM-5 and (b) thermogravimetric analysis of the spent catalysts at various temperatures of 300−450 °C with methanol WHSV values of 5 h^{-1} (300−325 °C) and 15 h^{-1} (350−450 °C). (c) GC−MS chromatograms of the retained organic species over the spent HZSM-5 and HZSM-5@S-1 zeolites after MTH reaction at 350 °C. It is worth mentioning that soluble "coke" contains some active aromatic species, e.g., polymethylbenzenes, that are retained on the spent zeolites.

reaction, but the active aromatic species age unavoidably into inactive PAHs, leading to deactivation.

Over 50 years of experimental and computational studies of MTH reaction,[39−42] PAHs as the deactivating species have been recognized but not unambiguously structurally identified, resulting in the mechanistic controversies of deactivation remaining ongoing. The traditional view posited that coke deposits covering the external surface were the main cause of HZSM-5 deactivation.[43,44] However, recently, the internal coke species were demonstrated to be more detrimental than the external ones.[26,42] Coke precursors (aromatic species) were found to be generated inside the channel intersections of HZSM-5, followed by ring-expansion growth along straight channels.[26,45] To decode the hidden molecular details and deactivation patterns, we reinterpret the deactivation behavior of the HZSM-5-catalyzed MTH reaction.

MTH Reaction and the Soluble "Coke" Analysis. To rule out the possible effect of the external coke, the external acid sites of HZSM-5 were selectively passivated by an in situ crystallized silicalite-1 layer. The obtained sample was labeled as HZSM-5@S-1. The physicochemical properties of HZSM-5 and HZSM-5@S-1 samples are presented in Figures S1, S2 and Table S1. After silicalite-1 deposition, almost no change in the XRD patterns indicated the maintenance of the MFI topological structure (Figure S2). No significant variations of specific surface areas and micropore volumes confirmed the nondestruction of silicalite-1 deposition (Table S1). The element distribution analysis by STEM-EDS showed that the silicalite-1 layer with a thickness of around 200 nm was relatively uniformly distributed on the outer surface of HZSM-5 zeolite (Figure S3).

MTH reactions over HZSM-5 and HZSM-5@S-1 at various temperatures of 300−450 °C are shown in Figures 2a and S4. Under low temperature (<350 °C), an obvious induction period was observed. The thermogravimetric analysis of the spent catalysts (Figure 2b) showed that the coke content was less than 6%. The coke deposits were released and analyzed by a GC−MS analysis. GC−MS chromatograms show that the retained coke molecules were mainly methylbenzene and methylnaphthalene species (Figure S5). Increasing the reaction temperature from 350 to 400 °C, there was an almost linear increase in the proportion of insoluble coke, and correspondingly, the proportion of soluble "coke" decreases linearly (Figure 2b). Concurrently, the retained organic species gradually transitioned from methylbenzene and methylnaphthalene species (at 300−325 °C) to three-ring PAHs species (at 350−375 °C) (Figure S5). Noticeably, at temperatures above 375 °C, the increasing trend of the coke amount slowed down, and the proportions of soluble "coke" and insoluble coke no longer changed apparently (Figure 2b). In parallel, the detectable soluble "coke" molecules by GC−MS decreased dramatically at 375−450 °C (Figure S5), suggesting the remarkable transformation of lighter, soluble "coke" (1−3 ring aromatics) into a heavier, insoluble one (i.e., the highly condensed PAHs).

A detailed structural analysis of the imprisoned organic species on the spent HZSM-5 and HZSM-5@S-1 zeolites is shown in Figure 2c. Regardless of whether silicalite-1 was deposited on the outer surface of HZSM-5, the soluble

https://doi.org/10.1021/jacs.5c10664
J. Am. Chem. Soc. 2025, 147, 41379−41389

Table 1. Molecular Composition of Coke Species Extracted from the Spent HZSM-5 after MTH Reaction at 450 °C[a]

Group	Unsaturation number	Formula	Carbon number	m/z range	Molecular structure
A	12	$C_{17}H_{12}+nCH_2$	18-23	231-301	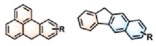
B	13	$C_{18}H_{12}+nCH_2$	18-23	229-299	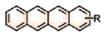
C	14	$C_{20}H_{14}+nCH_2$	20-23	255-297	
D	15	$C_{21}H_{14}+nCH_2$	20-26	253-337	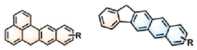
E	18	$C_{25}H_{16}+nCH_2$	25-29	317-373	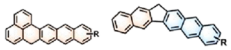
F	20	$C_{28}H_{18}+nCH_2$	28-32	355-411	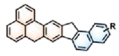
G	21	$C_{29}H_{18}+nCH_2$	28-33	355-423	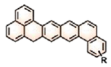
H	23	$C_{32}H_{20}+nCH_2$	32-38	405-489	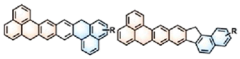
I	26	$C_{36}H_{22}+nCH_2$	36-42	455-539	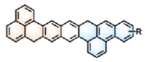
J	37	$C_{51}H_{30}+nCH_2$	52-57	657-727	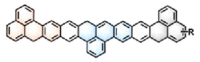
K	40	$C_{55}H_{32}+nCH_2$	55-62	693-791	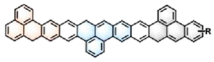

[a]Molecular structure of coke species (groups A−I) assigned from nc-AFM images. The heavier coke molecules (groups J and K) are inferred according to the imaged molecular structure and molecular growth regularity of coke species. For clarity, only coke molecules with the initial aromatic hydrocarbon structures are taken as illustrative examples. It should be noted that the CH_2 site has a large potential to be oxidized to a radical or a ketone group.

molecular species were almost consistent. This finding indicates that coke species on the outer surface are too heavy to be soluble in the solvent, thus not affecting the structural analysis of internal coke. In addition to the common aromatic species with 1−3 fused rings, biphenyl, methylfluorene, and methylene-bridged aromatic molecules were also detected, indicating the existence of a condensation growth route of two adjacent aromatic nuclei. These detected soluble coke molecules are mainly linear aromatic hydrocarbons, which conform to the 10-MR straight channels of the HZSM-5 zeolite.

Notable was the observed branched aromatic molecule, methylphenalene, as shown in Figure 2c. Its triangular-shaped configuration may enable it to be prone to occupying the channel intersections of HZSM-5. To verify this hypothesis, the tail gas of the MTH reaction was collected by CCl_4 absorption for 3 h and then analyzed by GC−MS. The chromatogram showed that tail gas mainly consisted of polymethylbenzene and polymethylnaphthalene species (Figure S6). No phenalene species were detected in the gaseous effluent. This observation implies that the bulky phenalene species fit in the channel intersections of HZSM-5, making it difficult for them to diffuse out. In this context, we can reasonably speculate that the occluded phenalene species may serve as key structural building blocks for the growth of PAHs.

Besides, some intermediate aromatic species with exocyclic saturated five- or six-membered rings (indan, tetralin, and dihydronaphthalene substances) were also detected in tail gas (Figure S6). This observation implies the olefin alkylation and ring expansion pathway of aromatic growth. Moreover, the appearance of polymethylnaphthalenes in tail gas indicates their good fluidity inside the channels of HZSM-5. We can surmise that the fluid methylnaphthalene species may diffuse nearby and condense with the occluded aromatic precursors, e.g., phenalene species and their extended derivatives, into more condensed PAHs.

MALDI FT-ICR MS Analysis of the Condensed PAH Molecules. GC−MS analysis has identified the molecular structures of soluble "coke" retained inside the micropores of HZSM-5. However, at temperatures above 375 °C, the insoluble counterparts (beyond the upper limit of GC−MS analysis) dominated the coke species (Figure 2b). The molecular elucidation of these more condensed PAHs remains a formidable challenge. The advanced high-resolution MALDI FT-ICR MS technique seems promising. Next, we adopt the MALDI FT-ICR MS technique to analyze these heavier PAHs on HZSM-5@S-1 zeolite.

https://doi.org/10.1021/jacs.5c10664
J. Am. Chem. Soc. 2025, 147, 41379−41389

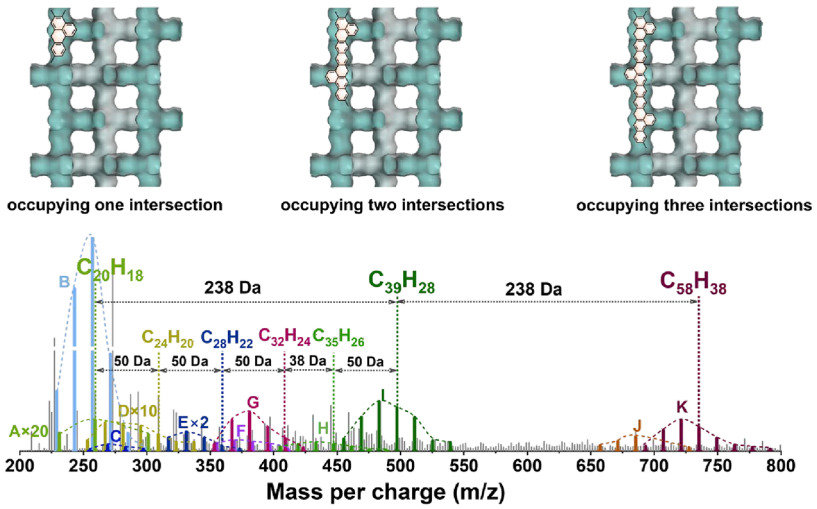

Figure 3. MALDI FT-ICR MS spectrum of the liberated coke deposits from the deactivated HZSM-5@S-1 after MTH reaction at 450 °C with a methanol WHSV of 2 h^{-1}. The illustrated molecular formulas correspond to the aromatic molecules with three methyl substitutions. Three sketch maps depict three representative coke molecules from groups A, I, and K that occupy one to three channel intersections of HZSM-5 zeolite. For clarity, only coke molecules with the initial aromatic hydrocarbon structures are taken as illustrative examples. It should be noted that the CH_2 site on triangular phenalene species and its derived hydrocarbons has a large potential to be oxidized to a radical or a ketone group.

MALDI FT-ICR MS analysis of the liberated coke deposits from the deactivated HZSM-5@S-1 after MTH reactions at 350 and 450 °C was performed. At 350 °C, the mass spectrum shows a pattern with a continuous distribution feature in the m/z range of 200−600 Da (Figure S7). At 450 °C, the mass spectrum can be divided into two clusters: 200−600 and 650−800 Da. The mass distribution in the m/z range of 200−600 Da was similar to the distribution at 350 °C. For simplification, the feature-rich spectrum within the m/z range of 200−600 Da was classified into nine groups (A−I) (Figure S7 and Table 1). The classification was based on the unsaturation number of the corresponding pristine aromatic counterparts of the imaged coke species by nc-AFM, as shown in Figure 4. The extracted MS peaks of the nine classified families of coke molecules are shown in Figure S8, which include the molecular composition and formula obtained through MS analysis and the imaged molecular structure by nc-AFM. The unsaturation number of coke molecules was linearly correlated with the carbon number in the range 12−26 (Figure S9).

Nine peak-groups were overlapped, and each group exhibited the characteristic of Gaussian-curved distributions of mass, characterized by the repeated mass increment of 14 Da (substitution of H- by CH_3- group). The complex mass pattern in the m/z range of 200−600 Da (between groups A and I) presented regular and repeated mass increments of 50 and 38 Da. Such mass intervals between the adjacent peak groups could be assigned to the building units of C_4H_2 (C_4 olefins) and C_3H_2 (C_3 olefins) that were attached to aromatic precursors, leading to the enlargement of aromatic rings. This observation implies the dominance of successive ring-expansion growth pathways of PAH molecules.

When the reaction temperature was increased to 450 °C, the mass range of coke deposits was extended to 650−800 Da (Figure 3), suggesting further mass growth of coke molecules. The mass spectral peaks in the m/z range of 650−800 Da can be classified into two groups (J and K) (Figure 3 and Table 1). The mass gap between the two clusters of 200−600 and 650−800 Da implied the condensation growth route, i.e., two adjacent aromatic precursors are condensed into a larger one. Noticeably, the m/z of groups A, I, and K differ regularly by 238 Da. This mass pattern enables us to speculate that coke molecules located in the neighboring channel intersections of HZSM-5 can be cross-linked across the channel, resembling the cage-passing growth mechanism on SAPO-34.[12] In summary, aromatic precursors formed inside the channel intersections can grow into the heavier homologues through the successive alkylation-cyclization-hydrogen transfer steps (with continuous mass distribution) and condensation route of the adjacent aromatics (with group-based structural characteristics).

The MALDI FT-ICR MS technique can provide rich structural information on the condensed PAHs with m/z of around 200 ∼ 1000 Da, bridging the analysis upper limit (<300 g/mol) of the traditional GC−MS method. The broad mass spectrum range for analyzing diverse PAHs, associated with the regular coke molecular architecture, makes it feasible to track the growth trajectory of coke molecules. However, due to the molecular diversity, the molecular structures inferred by the mass number of MALDI FT-ICR MS analysis are by no means conclusive. The presence of diverse isomers cannot be resolved. Next, by combining STM and nc-AFM techniques, we realized the single-molecule imaging of PAH molecules with detailed structural feature.

Single-Molecule Direct Imaging of Coke Deposits by Combining STM and nc-AFM. The coke deposits were liberated from the deactivated HZSM-5 zeolite after MTH reaction at 450 °C. After HF dissolution of the zeolite framework and CCl_4 solvent extraction, the insoluble coke deposits were collected through filtration. Then, they were transferred onto a SiC wafer and deposited onto an Au(111) substrate by flash-heating under ultrahigh vacuum conditions. A CO-functionalized tip was used to perform STM and nc-AFM imaging at 4 K, respectively.

STM image showed the morphology of coke molecules deposited on the Au(111) substrate (Figures S10 and S11). The intramolecular and intermolecular contrasts were almost uniform. Most of the coke molecules adopted a distinct bone-like morphology, which aligns well with the pore architecture

https://doi.org/10.1021/jacs.5c10664
J. Am. Chem. Soc. 2025, 147, 41379−41389

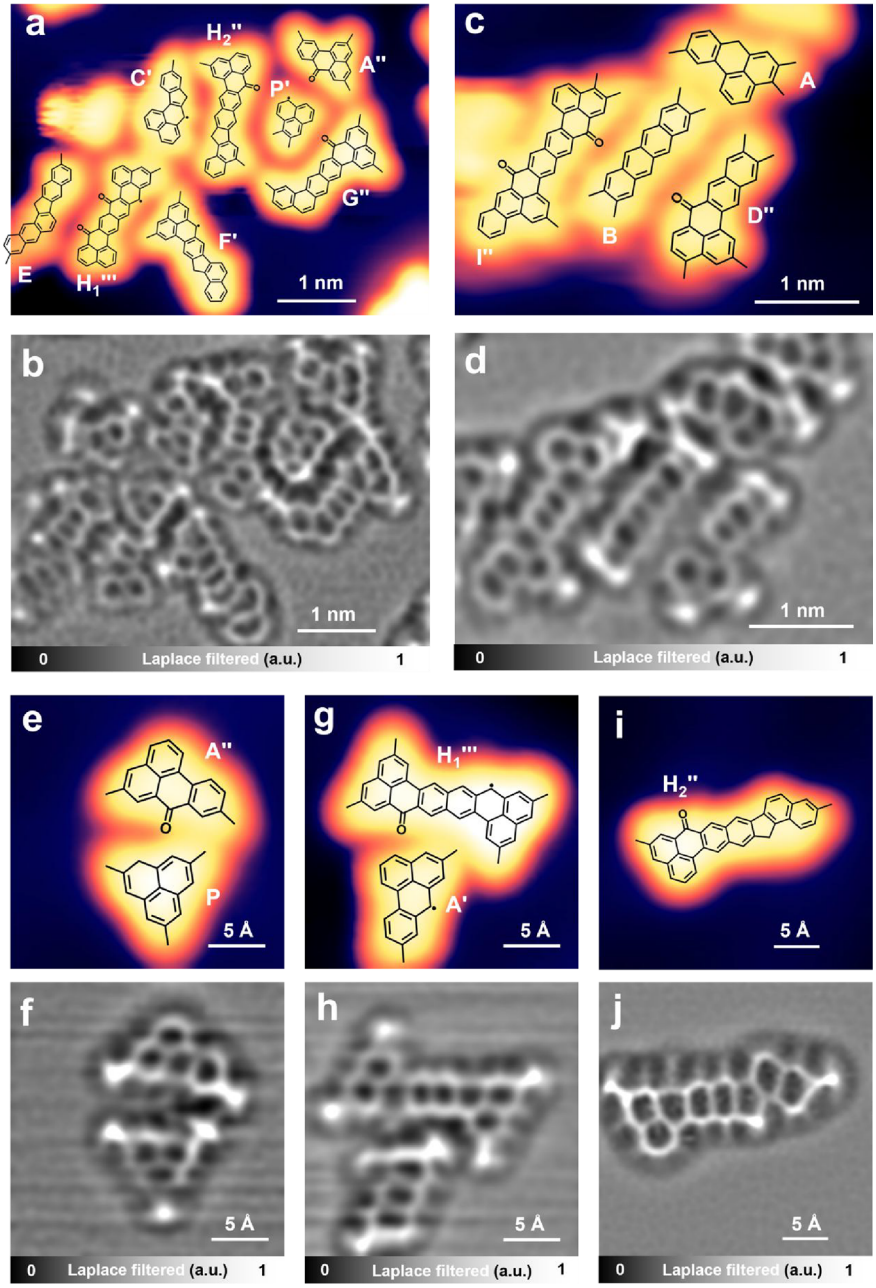

Figure 4. Direct imaging of coke species. (a, c) STM images and (b, d) the corresponding Laplace-filtered nc-AFM images of coke species collected from the spent HZSM-5 zeolite. (e, g, i) STM images and (f, h, j) the corresponding Laplace-filtered nc-AFM images of coke species collected from spent HZSM-5@S-1 zeolite. STM images were acquired at V_s = −300 mV, I_t = 20 pA. The nc-AFM images were acquired using a CO-functionalized tip under constant-height mode (A = 100 pm). The proposed molecular structures of the coke species are superimposed on the STM images. The depicted molecular structures represent one of the possible resonance forms of their pristine PAH molecules. The numbering of the imaged molecules is based on the unsaturation number of their pristine PAH molecules. The lower numbers 1 or 2 represent the different molecular structures with the same unsaturation number of their pristine PAH molecules; the upper symbols ′, ″, and ‴ represent the radical species, oxygen-containing species, and their mixture in one coke species. The bright spots can be classified into two categories of sites with nonplanar configurations: methyl groups outside the carbon skeleton and CH_2 units in the carbon skeleton.

of the HZSM-5 channel featuring "intersection-10 MR channel-intersection" topology, implying that these regularly shaped molecules were likely formed within the micropore of HZSM-5 zeolite.

Atomically resolved structures of individual coke molecules were then obtained via the combination of STM and nc-AFM imaging. Representative coke molecules extracted from the spent HZSM-5 after MTH reaction at 450 °C are shown in Figures 4a–d and S11. A variety of species, including PAHs, radicals, and oxidized aromatic hydrocarbons, were identified. It should be noted that the assignments of the radical site and oxygen site are not absolutely conclusive. What should be highlighted is the identification of the chemical reactivity of the CH_2 site in the traditionally viewed inert coke molecule and its evolution to the CH· and C═O sites. In light of the unsaturated number of their normal aromatic counterparts, the imaged molecules are classified into nine groups (A–I). These molecular structures serve as references for correlating the

https://doi.org/10.1021/jacs.5c10664
J. Am. Chem. Soc. 2025, 147, 41379−41389

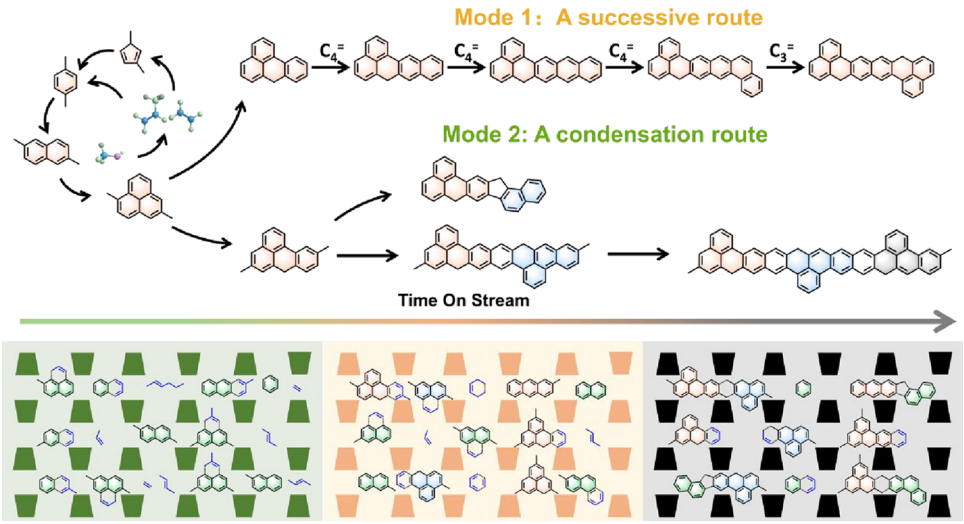

Figure 5. Growth routes of coke molecules on HZSM-5. The illustration depicts examples of the possible steps to propagate growth via a successive route and/or a condensation route and examples of evolving routes of coke species in HZSM-5 channels. For clarity, only coke molecules with the initial aromatic hydrocarbon structures are taken as illustrative examples. But it should be noted that the CH_2 site has a large potential to be oxidized to a radical or a ketone group.

STM and nc-AFM observations with MALDI FT-ICR MS results (Figures S7 and 3), enabling the assignments of the corresponding spectral peaks.

Heavier coke deposits with a mass range of 650−800 Da (Groups J and K in Figure 3) were not visualized by nc-AFM, likely due to the limitations in sample preparation, such as the difficulty in evaporating the highly condensed polycyclic species under current experimental conditions. Nevertheless, the structural evolution of the imaged molecules (groups A−I, in Figure 3 and Table 1) in combination with their spatial growth constraints inside zeolite micropores allows for the rational prediction of the molecular structures of such heavier coke species (Groups J and K) as proposed in Table 1.

The smallest species observed by nc-AFM were phenalene (molecule P), benzophenalene (molecule A), and their radical and oxidized derivatives with different methyl substitutions. The detection of methylphenalene in the retained soluble "coke" by GC−MS (Figure 2c) and its absence in tail gas effluent (Figure S5) provides compelling evidence that such species are trapped within the zeolite channel intersections. In this context, phenalene and benzophenalene, with their shapes like the ends of a bone, are identified as the basic structural units for PAHs growth. Once formed, phenalene and benzophenalene can continue to grow by successive alkylations with olefins along the 10-MR channel, across the adjacent channel intersection. They can also be condensed, by dehydrogenative coupling, with the adjacent aromatics (naphthalene, phenalene, benzophenalene, etc.) in the neighboring channel intersections. Eventually, more condensed PAHs are formed. The radical and oxidized aromatic species shown in Figure 4 are the derivatives of their normal counterparts. These two growth modes of PAHs are consistent with the mass spectral patterns, as shown in Figure 3.

In addition to the typical fused aromatic structures, there is also a kind of coke molecule linked by a five-membered ring unit (fluorene-based structure). These structures are thought to arise from condensation (dehydrogenative coupling) between two adjacent aromatic nuclei.[28] These two molecular growth routes of the condensed PAHs, i.e., a successive route and a condensation route, are also applicable for the lighter aromatic molecules, referring to the previous discussions on GC−MS analysis of the soluble "coke" and tail gas effluent, as shown in Figures 1c and S6. These results collectively suggest a unified mechanism picture of coke growth.

To rule out the possible effect of external coke, coke deposits collected from the coked HZSM-5@S-1 zeolite were also imaged by STM and nc-AFM, as shown in Figure 4e−j. The same structural motifs, including phenalene, benzophenalene, and their extended PAH derivatives, are identified. The consistency between the observed coke species on HZSM-5 and HZSM-5@S-1 confirms that the observed molecules originate primarily from the internal coke. In contrast, coke formed on the external surface of zeolite, lacking the spatial confinement, tends to grow freely into graphitized coke that is too heavy to be detected by means such as GC−MS, STM, and nc-AFM.

To summarize, as a complement to the traditional GC−MS method, the MALDI FT-ICR MS technique can monitor the molecule trajectories of coke deposits (with molecular weight up to ∼1000 g/mol) in light of the mass spectral pattern. However, due to the molecular diversity, MALDI FT-ICR MS cannot give precise molecular structures. STM and nc-AFM can resolve this problem by the direct imaging of coke molecules with precise structural determination. Nevertheless, single-molecule imaging gives finite molecular structures due to the sampling limit, making it difficult to realize the broad-range imaging of infinitely diverse coke molecules. Fortunately, molecular growth of coke species in a zeolite confined space is regular; nanoconfinement imparted by zeolite pores regulates the structural motifs and growth trajectories of PAHs. In these contexts, with the "structural code" decoded by nc-AFM, we can infer the unknown structures of the heavier coke species based on the imaged known molecules and their evolutionary pattern. By integrating the advantages of GC−MS, MALDI FT-ICR MS, as well as STM and nc-AFM, a spectrum of coke species ranging from soluble coke to insoluble coke with explicit atomic structures is realized. This achievement is difficult to achieve by any single technique.

Molecular Routes of Coke Deposits. Herein, we achieved the atomic-resolution structural identification of

https://doi.org/10.1021/jacs.5c10664
J. Am. Chem. Soc. 2025, 147, 41379−41389

coke species. This allows us to depict the molecular routes for mass growth of coke with a more well-defined molecular structure. Figure 5 shows examples of two classical growth routes of coke molecules on HZSM-5: a successive route (between aromatic precursors and olefins via alkylation-cyclization-hydrogen transfer steps) and a condensation route (between the adjacent aromatic precursors). According to the above discussions, both radical and oxidized species are derived from their normal aromatic hydrocarbons. For simplification, only the coke molecules with normal aromatic structures are taken as examples for illustration.

Coking of zeolites is a nucleation−growth process. Once incipient olefins are formed, they go through methylation/oligomerization-cyclization-hydrogen transfer reactions to form methylcyclopentenyl and polymethylbenzene species. The aromatic species can be taken as "nuclei/seeds" for coke growth. Polymethylbenzene species are then transformed into polyaromatic molecules (such as naphthalene, anthracene, phenalene, and benzophenalene species) occupying one channel intersection of HZSM-5. Phenalene and benzophenalene species, which have been identified as the key structural units, further propagate growth along the 10-MR channel to form more condensed PAHs occupying two channel intersections. Such molecular mass growth is achieved either through a successive route and/or through a condensation route with the neighboring aromatic precursors (such as phenalene or benzophenalene) in adjacent channel intersections. In the latter reaction stage, PAHs gradually block the channels, restricting the diffusion of reactants and active intermediates. The molecular routes of coke growth shift to the dominance of the condensation pathway, forming heavier PAHs occupying three or more intersections. Ultimately, the condensed PAHs and their radical and oxidized counterparts deactivate zeolite by covering the active sites and blocking the zeolite pores.

As the terminal product of the reaction, coke molecules match the pores of zeolites, and their growth routes are directly dictated by the pore architecture of zeolites. MALDI FT-ICR MS peaks of SAPO-34 showed discontinuous clustering with regular intervals.[12] While in addition to the regular intervals, MALDI FT-ICR MS peaks of HZSM-5 also exhibited continuous peaks in the low m/z range (Figure 3). Similar to the mode of cage-passing deactivation on SAPO-34,[12] channel intersection-passing deactivation mechanism (i.e., condensation between the neighboring aromatic precursors in adjacent channel intersections) is proposed on HZSM-5. The difference is that, unlike narrow 8-MR pore opening, the 10-MR channel of HZSM-5 makes the successive growth route more feasible. These results unravel the coke chemistry in zeolite confinements and demonstrate that coke growth is a shape-selective process.

Moreover, coke molecules with radical and oxygen-containing species were also visualized by nc-AFM, as shown in Figures 4 and S11. Figure S12 presents nc-AFM images of the exemplified benzophenalene molecule and its radical and oxidized counterparts, along with the discussion on the formation of radical and oxidized carbonaceous species. With this, we discerned the active structural sites on PAHs and supposed their varying chemical reactivity, in contrast to the previous view that PAHs in coke molecules are less reactive due to their aromatic character.[7−9] The identified radical and oxidized sites on coke species might behave as the initial sites for the ring-opening reaction during the regeneration process of the deactivated catalysts. Thus, this finding lays a molecular foundation for unraveling the regeneration mechanism of spent catalysts.

CONCLUSIONS

In this study, taking industrially relevant, HZSM-5-catalyzed, MTH as a model reaction, we identified molecular structures of coke species by integrating atomic-resolution STM and nc-AFM with GC−MS and MALDI FT-ICR MS techniques. A spectrum of coke molecules ranging from soluble to insoluble species with explicit molecular structures was identified. The structural identification provides molecular details of mechanistic routes. Phenalene and benzophenalene species, situated in the channel intersections of HZSM-5, were identified as the key structural building units for coke growth. Further molecular mass growth was realized either through a successive route (alkylation-cyclization-hydrogen transfer steps) or a condensation route (via fusing adjacent aromatic precursors), with the latter route being dominant in the later reaction stage. With this, a channel intersection-passing deactivation mechanism was proposed on HZSM-5, resembling the cage-passing deactivation mechanism on SAPO-34.[12] Besides radical and oxidized coke molecules were also directly imaged, expanding our molecular understanding of coke structures and laying a molecular foundation for unveiling the regeneration mechanism of the deactivated catalyst. This work resolved a long-standing puzzle of how to definitively identify the molecular structures of coke species. STM and nc-AFM techniques used here illustrate the great promise of being a powerful tool for mechanism exploration in catalysis science.

METHODS

Preparation of HZSM-5@S-1 Sample. Commercial H-ZSM-5 with a Si/Al ratio of 19 was provided by the Catalyst Factory of Nankai University. The external surface of HZSM-5 was coated with a silicalite-1 layer by the in situ crystallization method. The HZSM-5 sample was immersed in the solution with a molar composition of 1 SiO_2: 0.12 TPAOH: 30 EtOH: 230 H_2O, and was then subjected to continuous stirring for 3 h. The obtained suspension was transferred into a Teflon-lined stainless-steel autoclave and treated hydrothermally at 120 °C for 24 h. The collected solid products were thoroughly washed with deionized water three times and dried at 100 °C overnight. The resultant sample is herein designated as HZSM-5@S-1.

Characterization. STEM-EDS measurement was performed using a JEM-2100F instrument equipped with an energy dispersive spectrometer (EDS). STEM image was observed using a Hitachi TM 3000 scanning electron microscope at an acceleration voltage of 15 kV. Al and Si element distributions of HZSM-5@S-1 were measured by line and area scans at an acceleration voltage of 200 kV.

XRD patterns of the catalyst powder were obtained using a PANalytical X 'Pert PRO X-ray diffractometer, equipped with a Cu Kα radiation source (λ = 0.15418 nm) operating at 40 kV and 40 mA. The scanning speed was set at 2θ = 5.0° min^{-1}. XRD patterns were recorded at a 2θ range of 5° to 60°.

TGA was performed using an SDTQ 600 analyzer with a heating rate of 10 °C min^{-1} from room temperature to 900 °C in a flowing air atmosphere (100 mL min^{-1}). The weight loss below 250 °C was attributed to the desorption of physically adsorbed water.

The surface area and pore volume of fresh and deactivated catalysts were determined by nitrogen adsorption−desorption isotherms on a Micromeritics ASAP 2020 analyzer. The catalysts were first degassed under a vacuum at 350 °C for 4 h as a pretreatment to completely remove the adsorbed water. Adsorption−desorption data between p/p_0 = 0.05−0.2 were utilized to determine the specific surface area using the Brunauer−Emmett−Teller (BET) equation. The total pore

https://doi.org/10.1021/jacs.5c10664
J. Am. Chem. Soc. 2025, 147, 41379−41389

volume was calculated using the total amount of nitrogen adsorbed at p/p_0 = 0.972. The adsorption−desorption data at p/p_0 = 0.2 were utilized to calculate the external surface area, micropore area, and micropore volume using the *t*-plot method.

MTH Reaction Test. All MTH reactions were carried out at atmospheric pressure by using a fixed-bed quartz tube reactor with an inner diameter of 4 mm. The catalyst powder was extruded and sieved into 40−60 mesh particles. Before the reaction, the catalyst was activated for 1 h under a flow of N_2 at 450 °C, and then the temperature was set to the reaction temperature. CH_3OH (>99.99%) was carried into the reactor by N_2 through a saturated evaporator. The gaseous reaction products were kept at 200 °C to avoid condensation and were analyzed using an online GC−MS (Agilent 7890B/5977A) with a PLOT Q capillary column and a flame ionization detector (FID).

Liberating Coke Species from the Deactivated Catalysts. In the fume hood, the coke species were released by dissolution of the zeolite framework with a HF solution. Typically, 50 mg of the deactivated catalysts were dissolved in 0.5 mL of 40% HF solution in a Teflon vial. After the zeolite framework was totally digested and the unreacted HF was evaporated in the fume hood, the liberated coke species were extracted by 0.5 mL dichloromethane (CH_2Cl_2) or carbon tetrachloride (CCl_4). CH_2Cl_2 is used for the extraction of coke species for GC−MS analysis, while CCl_4 is used for the extraction of coke species for MALDI FT-ICR MS analysis.

After HF dissolution of the zeolite framework and CCl_4 solvent extraction, the insoluble fraction of coke deposits was collected through filtration and then carefully washed with CCl_4 to remove the absorbed organic substances. The collected coke powder was dried for STM and nc-AFM measurements.

GC−MS Analysis. GC−MS analysis was performed using an Agilent 7890A/5975C gas chromatograph equipped with an HP-5 capillary column and an FID detector. After HF dissolution of the zeolite framework, soluble coke species were extracted with CH_2Cl_2. Hexachloroethane (C_2Cl_6) was used as an internal standard to quantify the amount of soluble coke species.

MALDI FT-ICR MS Analysis. For MALDI FT-ICR MS measurements of coke species, the deactivated catalysts were dissolved in HF and then extracted with CCl_4. The coke species retained in the CCl_4 phase were tested after extraction. Then, 10 μL of the extracts was mixed with 10 μL of a THF solution with dithranol (5 mg mL^{-1} in THF) as the MALDI matrix. After sonication treatment, 1 μL of the mixture was spotted onto the sample holder and dried in air. The sample holder was then transferred into the ion source of the mass spectrometer for analysis. MS signals were recorded in a positive ion mode on a 15-T FT-ICR mass spectrometer (Solarix XR, Bruker Daltonics, Bremen, Germany) equipped with an Nd: YAG laser, emitting 355 nm laser to generate ions. The ion source parameters were optimized for a wide m/z range ($153 < m/z < 2000$). The ionization frequency was 200 Hz, and the grid width was 1000 μm.

EPR Measurement. Free radicals generated in the coke species were analyzed using a Bruker A200 at room temperature with a central magnetic field of 3250.00 G, a sweep width of 150.00 G, a sweep time of 30.00 s, a microwave power of 3.99 mW, a modulation amplitude of 1.000 G, and a conversion time of 40.0 ms. Two groups of samples were examined: liquid sample (using CH_2Cl_2 as solvent) and solid sample (5−10 mg of solid powder). Each sample was moved to a quartz tube with an inner diameter of 2 mm and then placed into the cavity of the EPR spectrometer for testing.

STM and nc-AFM Measurements. The collected coke powder was carefully transferred onto a clean SiC substrate. After cleaning the Au(111) surface by repeated Ar^+ sputtering and annealing at 400 °C, coke molecules were then sublimated to the Au(111) surface via the flash-heating method under ultrahigh vacuum conditions. The experiments were conducted by using a ScientaOmicron low-temperature STM/nc-AFM system operated with a Nanonis controller. The nc-AFM images were recorded in constant-height mode based on a qPlus sensor design[46] with f_0 = 46 kHz, $Q = 5 \times 10^4$, A = 100 pm. STM and nc-AFM images were processed with the Gwyddion software.

■ ASSOCIATED CONTENT

Supporting Information

The Supporting Information is available free of charge at https://pubs.acs.org/doi/10.1021/jacs.5c10664.

Characterization results (SEM, XRD, N_2 adsorption), GC−MS analysis of the retained organic species and tail gas, MALDI FT-ICR MS spectrum, STM image, discussion on the formation of radical and oxidized coke species, and other supplementary results (PDF)

■ AUTHOR INFORMATION

Corresponding Authors

Mengxi Liu − *CAS Key Laboratory of Standardization and Measurement for Nanotechnology, National Center for Nanoscience and Technology, Beijing 100190, China; University of Chinese Academy of Sciences, Beijing 100049, China;* orcid.org/0000-0001-7009-5269; Email: liumx@nanoctr.cn

Yuchun Zhi − *National Engineering Research Center of Lower-Carbon Catalysis Technology, Dalian National Laboratory for Clean Energy, Dalian Institute of Chemical Physics, Chinese Academy of Sciences, Dalian 116023 Liaoning, China;* orcid.org/0000-0003-1518-3930; Email: yuchunzhi@dicp.ac.cn

Zhongmin Liu − *National Engineering Research Center of Lower-Carbon Catalysis Technology, Dalian National Laboratory for Clean Energy, Dalian Institute of Chemical Physics, Chinese Academy of Sciences, Dalian 116023 Liaoning, China; University of Chinese Academy of Sciences, Beijing 100049, China;* orcid.org/0000-0002-7999-2940; Email: liuzm@dicp.ac.cn

Authors

Yingjun He − *National Engineering Research Center of Lower-Carbon Catalysis Technology, Dalian National Laboratory for Clean Energy, Dalian Institute of Chemical Physics, Chinese Academy of Sciences, Dalian 116023 Liaoning, China; University of Chinese Academy of Sciences, Beijing 100049, China*

Yi Zheng − *CAS Key Laboratory of Standardization and Measurement for Nanotechnology, National Center for Nanoscience and Technology, Beijing 100190, China; University of Chinese Academy of Sciences, Beijing 100049, China*

Yiyao Chen − *National Engineering Research Center of Lower-Carbon Catalysis Technology, Dalian National Laboratory for Clean Energy, Dalian Institute of Chemical Physics, Chinese Academy of Sciences, Dalian 116023 Liaoning, China; University of Chinese Academy of Sciences, Beijing 100049, China*

Jing Niu − *National Engineering Research Center of Lower-Carbon Catalysis Technology, Dalian National Laboratory for Clean Energy, Dalian Institute of Chemical Physics, Chinese Academy of Sciences, Dalian 116023 Liaoning, China*

Jingrui Chen − *CAS Key Laboratory of Standardization and Measurement for Nanotechnology, National Center for Nanoscience and Technology, Beijing 100190, China; University of Chinese Academy of Sciences, Beijing 100049, China*

Guoju Yang − *State Key Laboratory of Inorganic Synthesis and Preparative Chemistry, College of Chemistry, Jilin*

https://doi.org/10.1021/jacs.5c10664
J. Am. Chem. Soc. 2025, 147, 41379−41389

University, Changchun 130012, China; orcid.org/0000-0002-1691-4021

Wenna Zhang − *National Engineering Research Center of Lower-Carbon Catalysis Technology, Dalian National Laboratory for Clean Energy, Dalian Institute of Chemical Physics, Chinese Academy of Sciences, Dalian 116023 Liaoning, China*

Xianwen Zhang − *Dalian Institute of Chemical Physics, Chinese Academy of Sciences, Dalian 116023 Liaoning, China*

Shutao Xu − *National Engineering Research Center of Lower-Carbon Catalysis Technology, Dalian National Laboratory for Clean Energy, Dalian Institute of Chemical Physics, Chinese Academy of Sciences, Dalian 116023 Liaoning, China;* orcid.org/0000-0003-4722-8371

Wenfu Yan − *State Key Laboratory of Inorganic Synthesis and Preparative Chemistry, College of Chemistry, Jilin University, Changchun 130012, China;* orcid.org/0000-0002-1000-6559

Yingxu Wei − *National Engineering Research Center of Lower-Carbon Catalysis Technology, Dalian National Laboratory for Clean Energy, Dalian Institute of Chemical Physics, Chinese Academy of Sciences, Dalian 116023 Liaoning, China;* orcid.org/0000-0002-0412-1980

Xiaohui Qiu − *CAS Key Laboratory of Standardization and Measurement for Nanotechnology, National Center for Nanoscience and Technology, Beijing 100190, China; University of Chinese Academy of Sciences, Beijing 100049, China*

Complete contact information is available at: https://pubs.acs.org/10.1021/jacs.5c10664

Author Contributions

[#]Y.H. and Y.Z. contributed equally to this work.

Notes

The authors declare no competing financial interest.

■ ACKNOWLEDGMENTS

This work was financially supported by the National Key R&D Program of China (2024YFB4105401), the National Natural Science Foundation of China (22372164, 22288101, 22372048, 21790353, 21425310, and 22072148), the Youth Innovation Promotion Association of CAS (2022038), the CAS Project for Young Scientists in Basic Research (YSBR-054), and the Strategic Priority Research Program of Chinese Academy of Sciences (Grant No. XDB0770202).

■ REFERENCES

(1) Corma, A. Inorganic Solid Acids and Their Use in Acid-Catalyzed Hydrocarbon Reactions. *Chem. Rev.* **1995**, *95* (3), 559−614.

(2) Chen, L.; Sun, M.; Wang, Z.; Yang, W.; Xie, Z.; Su, B. Hierarchically Structured Zeolites: From Design to Application. *Chem. Rev.* **2020**, *120* (20), 11194−11294.

(3) Sun, M.; Zhou, J.; Hu, Z.; Chen, L.; Li, L.; Wang, Y.; Xie, Z.; Turner, S.; Van Tendeloo, G.; Hasan, T.; et al. Hierarchical Zeolite Single-Crystal Reactor for Excellent Catalytic Efficiency. *Matter* **2020**, *3* (4), 1226−1245.

(4) Gounder, R.; Iglesia, E. The catalytic diversity of zeolites: confinement and solvation effects within voids of molecular dimensions. *Chem. Commun.* **2013**, *49* (34), 3491−3509.

(5) Li, J.; Corma, A.; Yu, J. Synthesis of new zeolite structures. *Chem. Soc. Rev.* **2015**, *44* (20), 7112−7127.

(6) Fu, Q.; Bao, X. Confined microenvironment for catalysis control. *Nat. Catal.* **2019**, *2* (10), 834−836.

(7) Hwang, A.; Bhan, A. Deactivation of Zeolites and Zeotypes in Methanol-to-Hydrocarbons Catalysis: Mechanisms and Circumvention. *Acc. Chem. Res.* **2019**, *52* (9), 2647−2656.

(8) Martín, A. J.; Mitchell, S.; Mondelli, C.; Jaydev, S.; Pérez-Ramírez, J. Unifying views on catalyst deactivation. *Nat. Catal.* **2022**, *5* (10), 854−866.

(9) Fan, S.; Wang, H.; Wang, S.; Dong, M.; Fan, W. Recent progress in the deactivation mechanism of zeolite catalysts in methanol to olefins. *Sci. China Chem.* **2024**, *67* (12), 3934−3943.

(10) Sun, M.; Gao, S.; Hu, Z.; Barakat, T.; Liu, Z.; Yu, S.; Lyu, J.; Li, Y.; Xu, S.; Chen, L.; et al. Boosting molecular diffusion following the generalized Murray's Law by constructing hierarchical zeolites for maximized catalytic activity. *Natl. Sci. Rev.* **2022**, *9* (12), nwac236.

(11) Zhou, J.; Zhi, Y.; Zhang, J.; Liu, Z.; Zhang, T.; He, Y.; Zheng, A.; Ye, M.; Wei, Y.; Liu, Z. Presituated, "coke"-determined mechanistic route for ethene formation in the methanol-to-olefins process on SAPO-34 catalyst. *J. Catal.* **2019**, *377*, 153−162.

(12) Wang, N.; Zhi, Y.; Wei, Y.; Zhang, W.; Liu, Z.; Huang, J.; Sun, T.; Xu, S.; Lin, S.; He, Y.; et al. Molecular elucidating of an unusual growth mechanism for polycyclic aromatic hydrocarbons in confined space. *Nat. Commun.* **2020**, *11* (1), 1079.

(13) Guisnet, M.; Magnoux, P. Organic chemistry of coke formation. *Appl. Catal., A* **2001**, *212* (1), 83−96.

(14) Magnoux, P.; Roger, P.; Canaff, C.; Fouche, V.; Gnep, N. S.; Guisnet, M. New Technique for the Characterization of Carbonaceous Compounds Responsible for Zeolite Deactivation. *Stud. Surf. Sci. Catal.* **1987**, *34*, 317−330.

(15) Dai, W.; Wu, G.; Li, L.; Guan, N.; Hunger, M. Mechanisms of the Deactivation of SAPO-34 Materials with Different Crystal Sizes Applied as MTO Catalysts. *ACS Catal.* **2013**, *3* (4), 588−596.

(16) Hunger, M.; Weitkamp, J. In situ IR, NMR, EPR, and UV/Vis Spectroscopy: Tools for New Insight into the Mechanisms of Heterogeneous Catalysis. *Angew. Chem., Int. Ed.* **2001**, *40* (16), 2954−2971.

(17) Qian, Q.; Ruiz-Martínez, J.; Mokhtar, M.; Asiri, A. M.; Al-Thabaiti, S. A.; Basahel, S. N.; Weckhuysen, B. M. Single-catalyst particle spectroscopy of alcohol-to-olefins conversions: Comparison between SAPO-34 and SSZ-13. *Catal. Today* **2014**, *226*, 14−24.

(18) Chua, Y. T.; Stair, P. C. An ultraviolet Raman spectroscopic study of coke formation in methanol to hydrocarbons conversion over zeolite H-MFI. *J. Catal.* **2003**, *213* (1), 39−46.

(19) Signorile, M.; Rojo-Gama, D.; Bonino, F.; Beato, P.; Svelle, S.; Bordiga, S. Topology-dependent hydrocarbon transformations in the methanol-to-hydrocarbons reaction studied by operando UV-Raman spectroscopy. *Phys. Chem. Chem. Phys.* **2018**, *20* (41), 26580−26590.

(20) Guisnet, M.; Costa, L.; Ribeiro, F. R. Prevention of zeolite deactivation by coking. *J. Mol. Catal. A: Chem.* **2009**, *305* (1−2), 69−83.

(21) Mores, D.; Stavitski, E.; Kox, M. H. F.; Kornatowski, J.; Olsbye, U.; Weckhuysen, B. M. Space- and Time-Resolved In-situ Spectroscopy on the Coke Formation in Molecular Sieves: Methanol-to-Olefin Conversion over H-ZSM-5 and H-SAPO-34. *Chem.—Eur. J.* **2008**, *14* (36), 11320−11327.

(22) Whiting, G. T.; Nikolopoulos, N.; Nikolopoulos, I.; Chowdhury, A. D.; Weckhuysen, B. M. Visualizing pore architecture and molecular transport boundaries in catalyst bodies with fluorescent nanoprobes. *Nat. Chem.* **2019**, *11* (1), 23−31.

(23) Qian, Q.; Ruiz-Martínez, J.; Mokhtar, M.; Asiri, A. M.; Al-Thabaiti, S. A.; Basahel, S. N.; van der Bij, H. E.; Kornatowski, J.; Weckhuysen, B. M. Single-Particle Spectroscopy on Large SAPO-34 Crystals at Work: Methanol-to-Olefin versus Ethanol-to-Olefin Processes. *Chem.—Eur. J.* **2013**, *19* (34), 11204−11215.

(24) Schmidt, J. E.; Poplawsky, J. D.; Mazumder, B.; Attila, Ö.; Fu, D.; de Winter, D. A. M.; Meirer, F.; Bare, S. R.; Weckhuysen, B. M. Coke Formation in a Zeolite Crystal During the Methanol-to-Hydrocarbons Reaction as Studied with Atom Probe Tomography. *Angew. Chem., Int. Ed.* **2016**, *55* (37), 11173−11177.

(25) Schmidt, J. E.; Peng, L.; Poplawsky, J. D.; Weckhuysen, B. M. Nanoscale Chemical Imaging of Zeolites Using Atom Probe Tomography. *Angew. Chem., Int. Ed.* **2018**, *57* (33), 10422−10435.
(26) Wennmacher, J. T. C.; Mahmoudi, S.; Rzepka, P.; Sik Lee, S.; Gruene, T.; Paunović, V.; van Bokhoven, J. A. Electron Diffraction Enables the Mapping of Coke in ZSM-5 Micropores Formed during Methanol-to-Hydrocarbons Conversion. *Angew. Chem., Int. Ed.* **2022**, *61* (29), No. e202205413.
(27) Pinard, L.; Hamieh, S.; Canaff, C.; Ferreira Madeira, F.; Batonneau-Gener, I.; Maury, S.; Delpoux, O.; Ben Tayeb, K.; Pouilloux, Y.; Vezin, H. Growth mechanism of coke on HBEA zeolite during ethanol transformation. *J. Catal.* **2013**, *299*, 284−297.
(28) Chaouati, N.; Soualah, A.; Chater, M.; Tarighi, M.; Pinard, L. Mechanisms of coke growth on mordenite zeolite. *J. Catal.* **2016**, *344*, 354−364.
(29) Oteyza, D. G. D.; Gorman, P.; Chen, Y. C.; Wickenburg, S.; Riss, A.; Mowbray, D. J.; Etkin, G.; Pedramrazi, Z.; Tsai, H. Z.; Rubio, A. Direct imaging of covalent bond structure in single-molecule chemical reactions. *Science* **2013**, *340* (6139), 1434−1437.
(30) Zhang, J.; Chen, P.; Yuan, B.; Ji, W.; Cheng, Z.; Qiu, X. Real-Space Identification of Intermolecular Bonding with Atomic Force Microscopy. *Science* **2013**, *342* (6158), 611−614.
(31) Chen, P.; Metz, J. N.; Mennito, A. S.; Merchant, S.; Smith, S. E.; Siskin, M.; Rucker, S. P.; Dankworth, D. C.; Kushnerick, J. D.; Yao, N.; et al. Petroleum pitch: Exploring a 50-year structure puzzle with real-space molecular imaging. *Carbon* **2020**, *161*, 456−465.
(32) Schuler, B.; Meyer, G.; Peña, D.; Mullins, O. C.; Gross, L. Unraveling the Molecular Structures of Asphaltenes by Atomic Force Microscopy. *J. Am. Chem. Soc.* **2015**, *137* (31), 9870−9876.
(33) Schulz, F.; Maillard, J.; Kaiser, K.; Schmitz-Afonso, I.; Gautier, T.; Afonso, C.; Carrasco, N.; Gross, L. Imaging Titan's Organic Haze at Atomic Scale. *Astrophys. J. Lett.* **2021**, *908* (1), l13.
(34) Commodo, M.; Kaiser, K.; De Falco, G.; Minutolo, P.; Schulz, F.; D'Anna, A.; Gross, L. On the early stages of soot formation: Molecular structure elucidation by high-resolution atomic force microscopy. *Combust. Flame* **2019**, *205*, 154−164.
(35) Xu, S.; Zhi, Y.; Han, J.; Zhang, W.; Wu, X.; Sun, T.; Wei, Y.; Liu, Z. Advances in Catalysis for Methanol-to-Olefins Conversion. *Adv. Catal.* **2017**, *61*, 37−122.
(36) Svelle, S.; Joensen, F.; Nerlov, J.; et al. Conversion of Methanol into Hydrocarbons over Zeolite H-ZSM-5: Ethene Formation Is Mechanistically Separated from the Formation of Higher Alkenes. *J. Am. Chem. Soc.* **2006**, *128* (46), 14770−14771.
(37) Zhang, W.; Zhi, Y.; Huang, J.; Wu, X.; Zeng, S.; Xu, S.; Zheng, A.; Wei, Y.; Liu, Z. Methanol to Olefins Reaction Route Based on Methylcyclopentadienes as Critical Intermediates. *ACS Catal.* **2019**, *9* (8), 7373−7379.
(38) Lin, S.; Zhi, Y.; Chen, W.; Li, H.; Zhang, W.; Lou, C.; Wu, X.; Zeng, S.; Xu, S.; Xiao, J.; et al. Molecular Routes of Dynamic Autocatalysis for Methanol-to-Hydrocarbons Reaction. *J. Am. Chem. Soc.* **2021**, *143* (31), 12038−12052.
(39) Vogt, E. T. C.; Fu, D.; Weckhuysen, B. M. Carbon Deposit Analysis in Catalyst Deactivation, Regeneration, and Rejuvenation. *Angew. Chem., Int. Ed.* **2023**, *62* (29), No. e202300319.
(40) Müller, S.; Liu, Y.; Vishnuvarthan, M.; Sun, X.; van Veen, A. C.; Haller, G. L.; Sanchez-Sanchez, M.; Lercher, J. A. Coke formation and deactivation pathways on H-ZSM-5 in the conversion of methanol to olefins. *J. Catal.* **2015**, *325*, 48−59.
(41) Lezcano-Gonzalez, I.; Campbell, E.; Hoffman, A. E. J.; Bocus, M.; Sazanovich, I. V.; Towrie, M.; Agote-Aran, M.; Gibson, E. K.; Greenaway, A.; De Wispelaere, K.; et al. Insight into the effects of confined hydrocarbon species on the lifetime of methanol conversion catalysts. *Nat. Mater.* **2020**, *19* (10), 1081−1087.
(42) Lee, S.; Choi, M. Unveiling coke formation mechanism in MFI zeolites during methanol-to-hydrocarbons conversion. *J. Catal.* **2019**, *375*, 183−192.
(43) Bjørgen, M.; Svelle, S.; Joensen, F.; Nerlov, J.; Kolboe, S.; Bonino, F.; Palumbo, L.; Bordiga, S.; Olsbye, U. Conversion of methanol to hydrocarbons over zeolite H-ZSM-5: On the origin of the olefinic species. *J. Catal.* **2007**, *249* (2), 195−207.
(44) Wang, C.; Hu, M.; Chu, Y.; Zhou, X.; Wang, Q.; Qi, G.; Li, S.; Xu, J.; Deng, F. π-Interactions between Cyclic Carbocations and Aromatics Cause Zeolite Deactivation in Methanol-to-Hydrocarbon Conversion. *Angew. Chem., Int. Ed.* **2020**, *59* (18), 7198−7202.
(45) Brogaard, R. Y.; Weckhuysen, B. M.; Nørskov, J. K. Guest−host interactions of arenes in H-ZSM-5 and their impact on methanol-to-hydrocarbons deactivation processes. *J. Catal.* **2013**, *300*, 235−241.
(46) Giessibl, F. J. The qPlus sensor, a powerful core for the atomic force microscope. *Rev. Sci. Instrum.* **2019**, *90* (1), No. 011101.

https://doi.org/10.1021/jacs.5c10664
J. Am. Chem. Soc. 2025, 147, 41379−41389